Powder Technology 421 (2023) 118439

Contents lists available at ScienceDirect

Powder Technology

journal homepage: www.journals.elsevier.com/powder-technology

Modeling simultaneous particle shrinkage, dissolution and breakage using the modified moving grid technique

Simon Ing Xun Tiong [a], Firnaaz Ahamed [b], Hariswaran Sitaraman [c], Suet Lin Leong [a], Yong Kuen Ho [a,d,*]

[a] Chemical Engineering Discipline, School of Engineering, Monash University Malaysia, Jalan Lagoon Selatan, Bandar Sunway, 47500, Selangor, Malaysia
[b] Department of Biological Systems Engineering, University of Nebraska-Lincoln, Lincoln, NE, USA
[c] Computational Science Center, National Renewable Energy Laboratory, 15013 Denver West Parkway, Golden, CO 80401, USA
[d] Monash-Industry Plant Oils Research Laboratory, Monash University Malaysia, Jalan Lagoon Selatan, Bandar Sunway, 47500, Selangor, Malaysia

HIGHLIGHTS

- Non-mass conserving fragmentation problem is solved by a modified Moving Grid Technique (m-MGT).
- Shrinkage of particles is mimicked using a continuous left moving grid.
- Disappearance or dissolution of particles is represented by removing bins routinely.
- Such modifications accurately capture the dynamics of concurrent mass-decreasing and number-reducing fragmentation system.

GRAPHICAL ABSTRACT

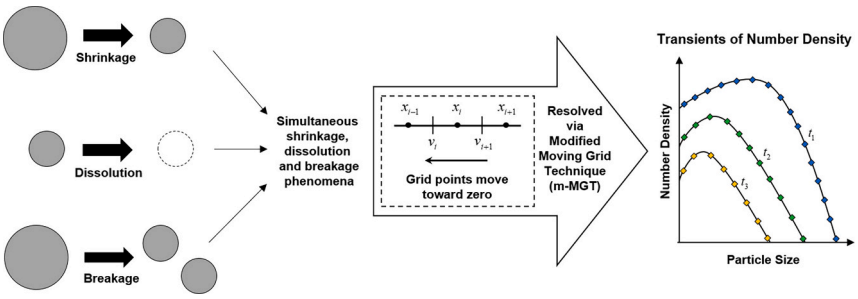

ARTICLE INFO

Keywords:
Population balances
Moving grid
Shrinkage
Dissolution
Breakage
Grid removal

ABSTRACT

Simultaneous shrinkage, dissolution and breakage are important particle size reduction phenomena that characterize processes like the reactive degradation of solid chemicals. The dynamics of the particle size distribution (PSD) for such processes are non-trivial to model due to the number expending processes brought about by the eventual dissolution of particles. To this end, Population Balance Model (PBM) resolved through the sectional techniques is the natural approach. Here, we introduce a modified Moving Grid technique (m-MGT) to accurately resolve the particle size reduction phenomena. Our technique mimics the perpetual particle shrinkage through a continuously left-moving size grid and incorporates a strategic grid removal routine to capture the disappearance of particles. Coupled with the Fixed Pivot (FP) discretization for breakage, our m-MGT not only preserves the moment-related properties, but also benchmarked very well against the analytical number densities and exhibited a minimum of first-order convergence in all assessed case studies.

* Corresponding author at: Chemical Engineering Discipline, School of Engineering, Monash University Malaysia, Jalan Lagoon Selatan, Bandar Sunway, 47500, Selangor, Malaysia.
E-mail address: ho.yongkuen@monash.edu (Y.K. Ho).

https://doi.org/10.1016/j.powtec.2023.118439
Received 27 December 2022; Received in revised form 15 February 2023; Accepted 7 March 2023
Available online 9 March 2023

1. Introduction

The co-occurrence of breakage, shrinkage, and dissolution is commonly encountered across various processes e.g., degradation of magnesium hydroxide solids [1], pharmaceutical compounds [2,3] and non-porous ores [4], combustion of coal char particles [5], and degradation of cellulose particles [6]. While breakage is a mass-conserving phenomenon, shrinkage is a number-conserving mass loss process, and dissolution results in the instantaneous disappearance of particles as their sizes reduce to zero (complete dissolution), leading to a steady decline in the total number of particles and mass of the system. The use of predictive dynamic models can facilitate the fundamental understanding and optimizations of such systems, but their necessary account for the mass- and number- expending processes is hindered by the complexities that arise from the combination of the individual but intertwined processes (i.e., breakage, shrinkage, and dissolution).

Multiple findings have attributed shrinkage (and, by extension, dissolution) as the primary determinant for breakage [5,7–9], but the sophistication of their interdependency is often overlooked in previous studies [3]. Furthermore, existing literature has treated the dissolution process as a combination of different mechanisms. For instance, Zhao, Jama, Buffo and Alopaeus [1] represented dissolution as a process purely defined by negative nucleation (i.e., instantaneous disappearance of particles), while other recent studies included the breakage phenomenon [1–4]. Moreover, particulate processes are often polydispersed in nature, and the use of an averaged quantity can lead to errors in modeling the system behavior [10].

To model the temporal evolution of the number density of dispersed phase entities, Population Balance Modeling (PBM) is the natural approach. Due to the partial integro-differential nature of Population Balance Equations (PBEs), generalized analytical solutions are a rare find and exist only for specific cases. Thus, the use of numerical solutions is often necessary. For mass-conserving breakage, sectional techniques such as the Fixed Pivot (FP) technique [11–14], Cell Average technique (CAT) [14,15] and Finite Volume schemes (FVS) [16–21] have been used. While PBM is commonly used for simultaneous growth, nucleation, and aggregation [22–30], as well as pure breakage systems, numerical techniques for simultaneous breakage, shrinkage, and dissolution are limited. A handful of studies solved PBEs accounting for shrinkage alone in the form of a negative growth using the Method of Moments (MOM) [31,32] and finite differences [1,2], while others considered simultaneous shrinkage and breakage through extended quadrature MOM [33], the technique based on Moving Pivot Technique and CAT [34], and the MOM-based moment projection technique [35].

Although MOM and its variants are simple, computationally inexpensive, and capable of estimating the desired moment-based properties with high accuracy, the techniques are not designed to capture the dynamics of the entire particle size distribution and require the use of additional processing methods (which might incur inaccuracies) to reconstruct the number distribution. Additionally, the finite differences are inadequate in solving PBEs involving convective terms (i.e., shrinkage) due to numerical diffusion [30]. In this regard, relatively uninhibited from the aforementioned shortcomings, sectional techniques are suitable choices as they preserve a selected number of moment-based properties whilst tracing the complete number density with reasonable accuracy and computational efficiency. The Moving Grid technique developed by Kumar and Ramkrishna [30] is, especially, an appealing strategy to resolve PBEs with a convective term given that it allows the preservation of any two integral properties of interest and is free from numerical dispersion via the use of a time adaptive grid. However, the technique was originally devised for size-expanding phenomena (i.e., simultaneous growth, nucleation and aggregation), and to resolve the complete opposite of size reduction phenomena entails additional complexities. Although the Moving Grid technique was previously applied to model the dissolution of particles, the necessary numerical algorithm to account for the concomitant breakage phenomenon was absent [36].

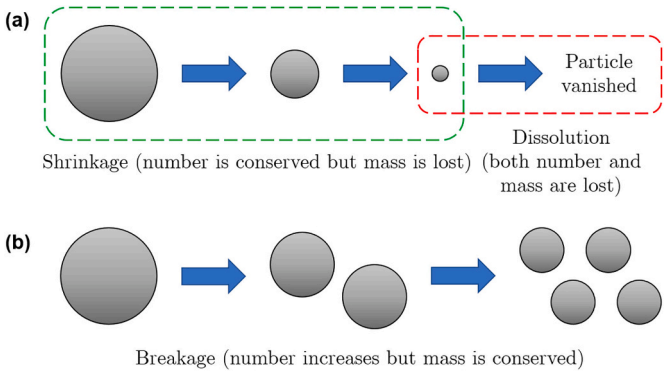

Fig. 1. Illustration of (a) the continuous mass removal phenomenon, and (b) the breakage phenomenon.

In this work, we introduce a modified Moving Grid technique (m-MGT) to solve the simultaneous shrinkage, dissolution, and breakage problem, which is the crux of various solid degradation processes. We model the particle size reduction due to convective process using a left-moving grid, which however poses a problem that is not encountered in the cases of particle size expansion. The grid points will eventually coincide at zero, and then move past zero and finally travel into the negative domain in this fashion. Thus, as a key feature, we include a rational bin-discarding strategy to resolve the problem of the left-moving grid crossing over into the negative domain due to size reduction. Further, we also examine the potential of our m-MGT in handling asymptotic cases where shrinkage is more dominant over breakage and vice versa. Our m-MGT which exhibits at least first order grid convergence not only enables an accurate prediction of the number density, but also the important moments across various case studies assessed. The organization of this paper is as follows. Section 2 presents the theoretical framework of the m-MGT. Following this, we validate the performance of the m-MGT against the analytical solutions for various cases and also study its order of convergence in Section 3. Conclusions to this study are presented in the final section.

2. Theoretical framework

2.1. Conceptual description of breakage, shrinkage, and dissolution

As alluded to previously, shrinkage and dissolution take place jointly, whereby a particle of a finite size shrinks until its size is reduced to zero and vanishes from the system. Shrinkage causes mass loss but conserves the number, whereas dissolution causes the loss of both mass and number (Fig. 1a). Conversely, breakage conserves the total mass of the system but not the number of particles (Fig. 1b). The simultaneous shrinkage, dissolution and breakage phenomenon is essentially the opposite of the simultaneous growth, nucleation and aggregation process for which the Moving Grid technique was initially developed, and we effectively adapt the technique via the m-MGT to reasonably account for the former as shown in the following section.

2.2. General formulation of simultaneous breakage, shrinkage, and dissolution population balances

A well-mixed batch dimensionless PBE to model simultaneous shrinkage, dissolution and breakage with particle size as the sole internal coordinate is given as [8]:

$$\frac{\partial n(v,t)}{\partial t}+\frac{\partial}{\partial v}[c(v)n(v,t)]=\int_{v}^{\infty}\beta(v,w)\Gamma(w)n(w,t)dw-\Gamma(v)n(v,t) \tag{1}$$

Here, $n(v,t)$ is the continuous number density and the second term on the

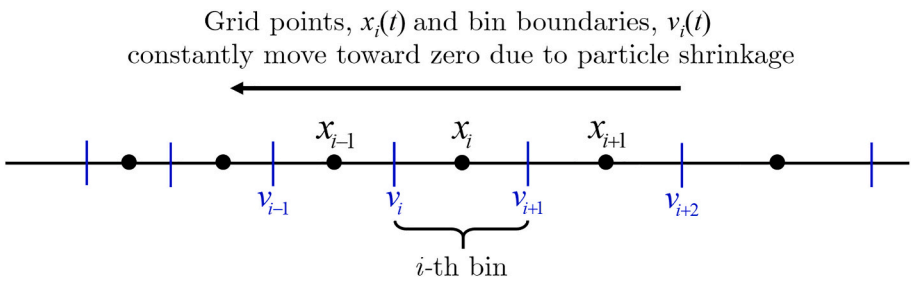

Fig. 2. A moving grid for particle size reduction with shrinkage. Here, $x_i = (v_{i+1} + v_i)/2$ is the grid point for the i-th bin bounded by $[v_i, v_{i+1}]$.

left-hand side (LHS) represents the shrinkage of particles of size v, where $c(v)$ is the shrinkage rate. Conversely, the terms on the right-hand side (RHS), following their sequence of appearance, describe the birth of particles of size v due to the breakage of particles of size $w \geq v$ and the death of the particles of size v due to their breakage into smaller particles, where $\beta(v,w)$ is the stoichiometric kernel which governs the formation of particles of size v and $w - v$ from w and $\Gamma(v)$ is the breakage rate. Although dissolution is not explicitly apparent in Eq. (1), the continuous disappearance of particles with a finite mass occurs as their sizes shrink to zero. As such, dissolution can be incorporated as a boundary condition in Eq. (1), i.e., $n(0,t) = 0$. For convenience, all quantities in Eq. (1) and in the texts that follow are presented in dimensionless form, with the omission of the term 'dimensionless' or special symbols for clarity and coherence. We choose to present the theoretical framework in the dimensionless form because the non-dimensionalization of PBE with general power law rates leaves the PBE virtually unchanged, except that all variables are now dimensionless. Thus, the general implementation of the numerical scheme remains unaffected. Interested readers may refer to Appendix A for the non-dimensionalization of the PBE.

2.3. Sectional technique solutions to simultaneous breakage, shrinkage, and dissolution population balances

Following a similar formulation as the Moving Grid technique presented by Kumar and Ramkrishna [30], shrinkage is dealt with using the method of characteristics and breakage is separately treated by the FP technique. Discretizing Eq. (1) (cf., Appendix B for details) yields:

$$\frac{dN_i(t)}{dt} = \sum_{k=i}^{M} \eta_{ik}\Gamma_k N_k(t) - \Gamma_i N_i(t) \tag{2}$$

where N_i is the total number of particles in the i-th bin, M is the final bin in the particle size domain. To obtain the average number density n_i for the i-th bin, we have $n_i = N_i/(v_{i+1} - v_i)$ by applying the mean value theorem on $N_i(t) = \int_{v_{i+1}}^{v_i} n(v,\, t)dv$. In addition, η_{ik} is the fractional

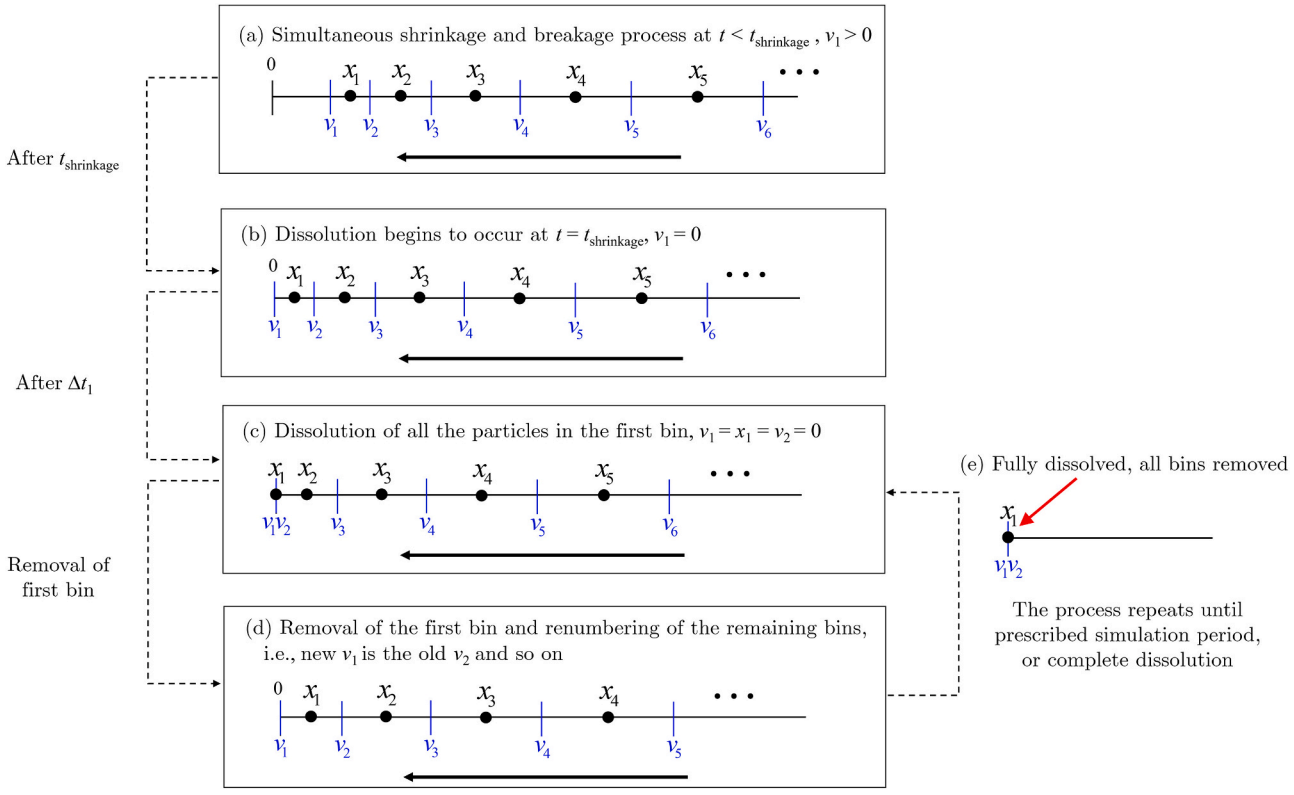

Fig. 3. Illustration of the step-wise moving grid strategy when dissolution of particles is involved: (a) moving grid for general shrinkage without dissolution, where the lower boundary of the first bin $v_1 > 0$ at $t < t_{\text{shrinkage}}$, (b) dissolution commences when $v_1 = 0$ at $t = t_{\text{shrinkage}}$, and the velocity is constrained to dv_1/dt to avoid movement of the bin into the negative domain, (c) complete dissolution of the first bin is achieved when the upper boundary $v_2 = 0$, and (d) removal of the first bin due to the complete dissolution and renumbering of the remaining bins, (e) removal of all the bins if the simulation time is equal or larger than the time at which 100% of the initial mass of the system is being removed, i.e., $t_{100\%}$.

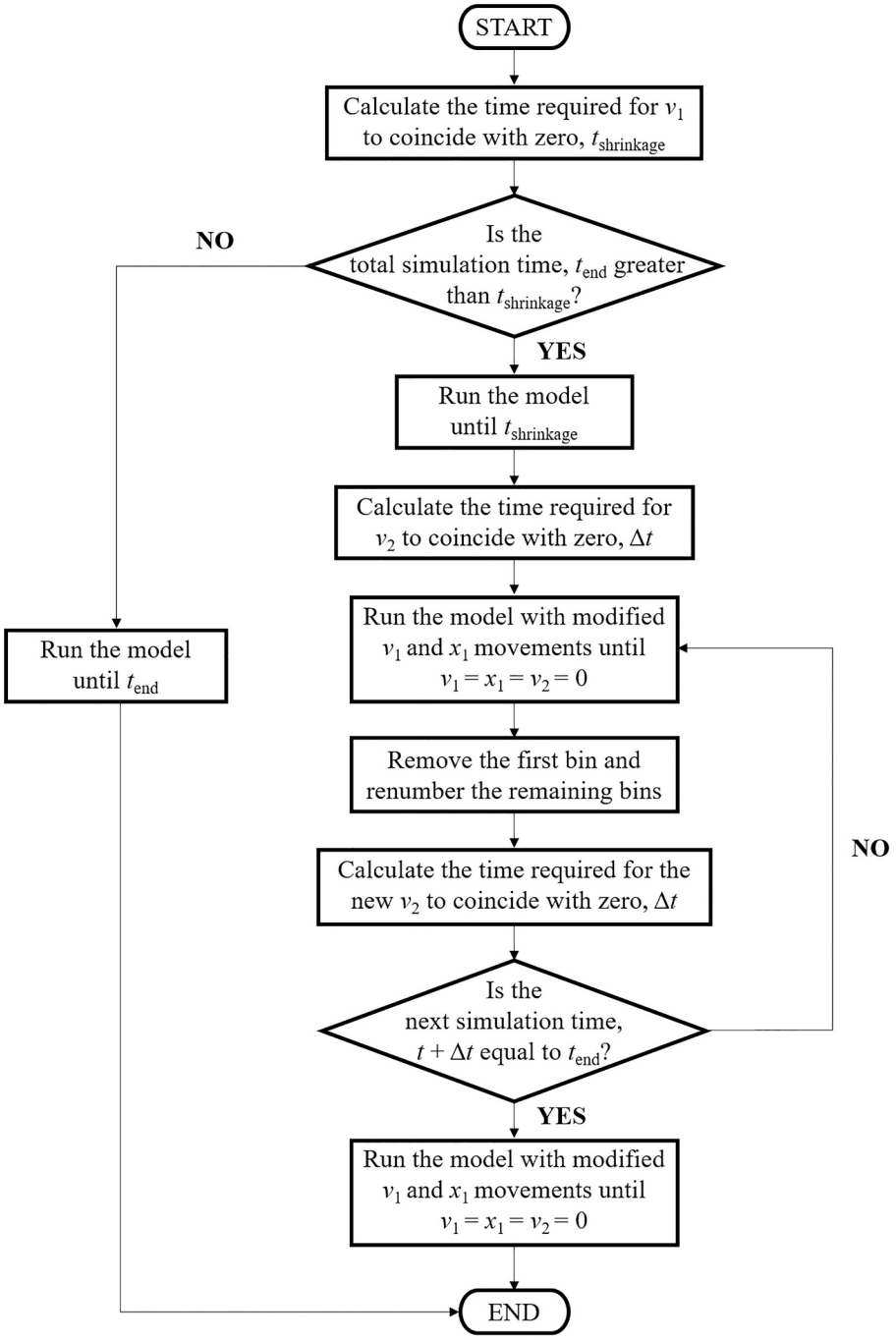

Fig. 4. Flowchart of m-MGT simulation.

allocation of particles due to breakage, where the choices of the preservation of the zeroth and the first moments (total number and mass, respectively) in the FP lead to:

$$\eta_{ik} = \int_{x_i}^{x_{i+1}} \left[\frac{x_{i+1} - v}{x_{i+1} - x_i}\right] \beta(v, x_k)\, dv + \int_{x_{i-1}}^{x_i} \left[\frac{v - x_{i-1}}{x_i - x_{i-1}}\right] \beta(v, x_k)\, dv \tag{3}$$

Here, x_i is the representative size (or grid point) for the i-th bin along the continuous particle size domain, $\beta(v, x_k)$ is the stoichiometric kernel for the formation of daughter particles from the breakage of parent particles with the size of x_k. Concomitantly, shrinkage is accounted for through the following:

$$\frac{dv_i}{dt} = c(v_i) \tag{4}$$

which implies that the bin boundaries move with time. It follows that the grid points which portray the representative sizes also travel at the particle shrinkage velocity:

$$\frac{dx_i}{dt} = c(x_i) \tag{5}$$

In this work, for simplicity, we write the grid-specific variables, e.g., $x_i(t)$ and $v_i(t)$ as x_i and v_i. Suffice to note that all grid-specific variables are functions of time due to the moving grid. A moving grid for problems with shrinkage is illustrated in Fig. 2, where the grid points and the bin boundaries constantly move to the left (toward zero) due to the continuous particle size reduction. It is worth mentioning that based on our meshing configuration, the time-dependent x_i can also be obtained

by averaging the results of Eq. (4), i.e., via $x_i = (v_{i+1}+v_i)/2$. The system of equations given by Eqs. (2)–(5) can be readily resolved via any commercial ODE solvers. As a summary, Eqs. (2)–(5) are applicable for a general case of simultaneous shrinkage, dissolution, and breakage, which are readily amenable to model different scenarios (e.g., pure shrinkage, with/without dissolution) through simplifications or special treatments.

The association of our approach with the technique originally devised by Kumar and Ramkrishna [11] ends here. Unlike the indefinite movement of particle sizes (grids) toward positive infinity to accommodate persisting growth and the addition of bins to account for nucleation, special provisions are needed to exclusively treat the dissolution phenomenon to avoid grids crossing over to the negative domain. In the following section, we discuss our moving grid strategy (m-MGT) to overcome the foregoing shortcoming encountered in the case of perpetual shrinkage and dissolution.

3. Results and discussion

3.1. Modified moving grid technique (m-MGT) to accommodate simultaneous breakage, shrinkage, and dissolution

As alluded to in the foregoing sections, particles are considered completely dissolved when their sizes reduce to zero. However, indefinite shrinkage will cause the particle sizes (representative grids) in our population balance formulation to cross over to the negative domain. Taking a cue from Kumar and Ramkrishna [30], we resolve the issue by removing the bins crossing over to the negative domain one at a time at predetermined intervals. Assuming the process begins with sizes of all particles in the system larger than zero (Fig. 3a), dissolution happens when the lower boundary of the first bin arrives at $v_1 = 0$ due to steady shrinkage (Fig. 3b). Given the shrinkage rate (velocity of x_i and v_i), the time required for v_1 to reach zero, i.e., $t_{\text{shrinkage}}$, can be computed via the following integral:

$$\int_0^{t_{\text{shrinkage}}} dt = \int_{v_1(0)}^{0} c(v_1)dv \tag{6}$$

From this juncture onwards, both grid points and bin boundaries will continue to move over to the negative domain without any special prescriptions. To resolve this issue, we handle the movement of v_1 and x_1 separately, where any further movement of v_1 is constrained by setting its velocity to zero:

$$\frac{dv_1}{dt} = 0 \tag{7}$$

As a result of this constraint, the movement of x_1 (which has not reached size zero) computed using the routine given by Eq. (4) will shift away from the midpoint of the first bin. Therefore, we alternatively assign the velocity for x_1 to remain as midpoint:

$$\frac{dx_1}{dt} = \frac{1}{2}\left(\frac{dv_1}{dt} + \frac{dv_2}{dt}\right) \tag{8}$$

The above expression is analogous to the equation given by Kumar and Ramkrishna [30] to ensure the grid points remain in the middle of the newly created bin during nucleation. Subsequently, Eqs. (2)–(5) along with Eqs. (7) and (8) are solved for a time interval Δt_1 until the upper boundary of the first bin arrives at zero, i.e., $v_2 = 0$. The time Δt_1 is identified in a way similar to Eq. (6), i.e., $\int_{t_{shrinkage}}^{t_{shrinkage}+\Delta_{t_1}} dt = \int_{v_2}^{0} c(v_2)dv$. We remove the first bin when $v_1 = x_1 = v_2 = 0$, that is, the population of particles contained in the first bin (N_1) is completely dissolved (Fig. 3c), and re-enumerate the remaining bins (Fig. 3d). Upon re-enumeration of the bins, it shall be understood that the time interval for the new v_2 to coincide with zero, i.e., Δt_2, will be different from Δt_1. As such, the time duration to remove the m-th bin on the initial grid can be computed using the following general expression:

Table 1
Implications of different shrinkage functions.

Shrinkage function	Implication
Linear rate, $c(v) = -v$	Dissolution is absent, $\gamma = 1$
Constant rate, $c(v) = -1$	Dissolution is present, $\gamma = 0$
Power law rate, $c(v) = -v^{\gamma}$	Dissolution is absent if $\gamma \geq 1$
	Dissolution is present if $\gamma < 1$

$$\int_{t_{\text{shrinkage}}+\sum_m \Delta t_{m-1}}^{t_{\text{shrinkage}}+\sum_m \Delta t_m} dt = \int_{v_2}^{0} c(v_2)dv \tag{9}$$

where v_2 here refers to the value of the upper boundary of the first bin on the current grid when the latest v_1 is zero. Moreover, it is crucial to point out that the bin discarding strategy intrinsically neglects the events occurring in the first bin during every Δt_m ($m = 1, 2, 3, \ldots$), i.e., the birth of small particles into the first bin due to the breakage of larger particles and partial dissolution of the particles in the first bin due to contraction of the bin. However, this is not an issue when a reasonably fine grid is employed because the dynamics of the system can be accurately captured at the end of every small Δt_m. In general, the steps are repeated after removal of each bin until the prescribed simulation time. If the prescribed simulation period is equal or larger than the time at which 100% of the initial mass of the system is depleted, i.e., $t_{100\%}$, all bins will be exhausted, indicating the complete dissolution of the system (Fig. 3e). The simulation procedure is summarized in Fig. 4.

3.2. Case studies

The theoretical framework presented in the foregoing sections is general and are amenable to visualize various scenarios. We explore different set-ups by adopting several classical power-law rates for shrinkage and breakage: (i) $\Gamma(v) = v^{\alpha}$ (breakage rate), (ii) $c(v) = -\varepsilon v^{\gamma}$ (shrinkage rate in the presence of breakage), and (iii) $c(v) = -v^{\gamma}$ (shrinkage rate in the absence of breakage). Here, ε is a constant that governs the relative extent of shrinkage to breakage [5,8], whereas α and γ are the exponents of breakage and shrinkage rates respectively. The implications of different forms of shrinkage functions on dissolution for breakage absence cases are summarized in Table 1 and explored further in subsequent sections. It shall be noted that the implication of the power law rate is based on our empirical observations.

To showcase the performance of our m-MGT on various scenarios involving shrinkage, we benchmark the numerical solutions against case-specific analytical solutions. We employ an exponential initial condition as follows for the simulations:

$$n_0(v) = \frac{N_0}{v_{0,i}} exp\left(\frac{-v}{v_{0,i}}\right) \tag{10}$$

The number density at the small size ranges is significant in such a distribution. Thus, the validity of the bin-discarding strategy can be assured if it accurately captures the change in the total number of particles, i.e., the zeroth moment. Here, N_0 is the initial number of particles and $v_{0,i}$ is the mean size of the initial particle size distribution. We set the values of N_0 and $v_{0,i}$ at 10 and configured a grid with initial minimum and maximum particle sizes set to $v_1 = 10^{-5}$ and $v_{M+1} = 500$, respectively, such that it covers most of the particles (i.e., > 99% by mass) prescribed by the initial condition given in Eq. (10). To avoid floating-point error, we arbitrarily select a threshold size of 1×10^{-8} as the point of dissolution, which is three orders of magnitude smaller than the initial v_1. Further, a typical geometric grid with 100 initial grid points and a geometric ratio, $r = 1.1940$ is employed. We utilize the foregoing initial condition and mesh configuration for all case studies featured in this work. As moment predictions are significant performance indicators of numerical techniques in preserving key characteristics of the system, we present moments of the population for all simulations, where the k-th

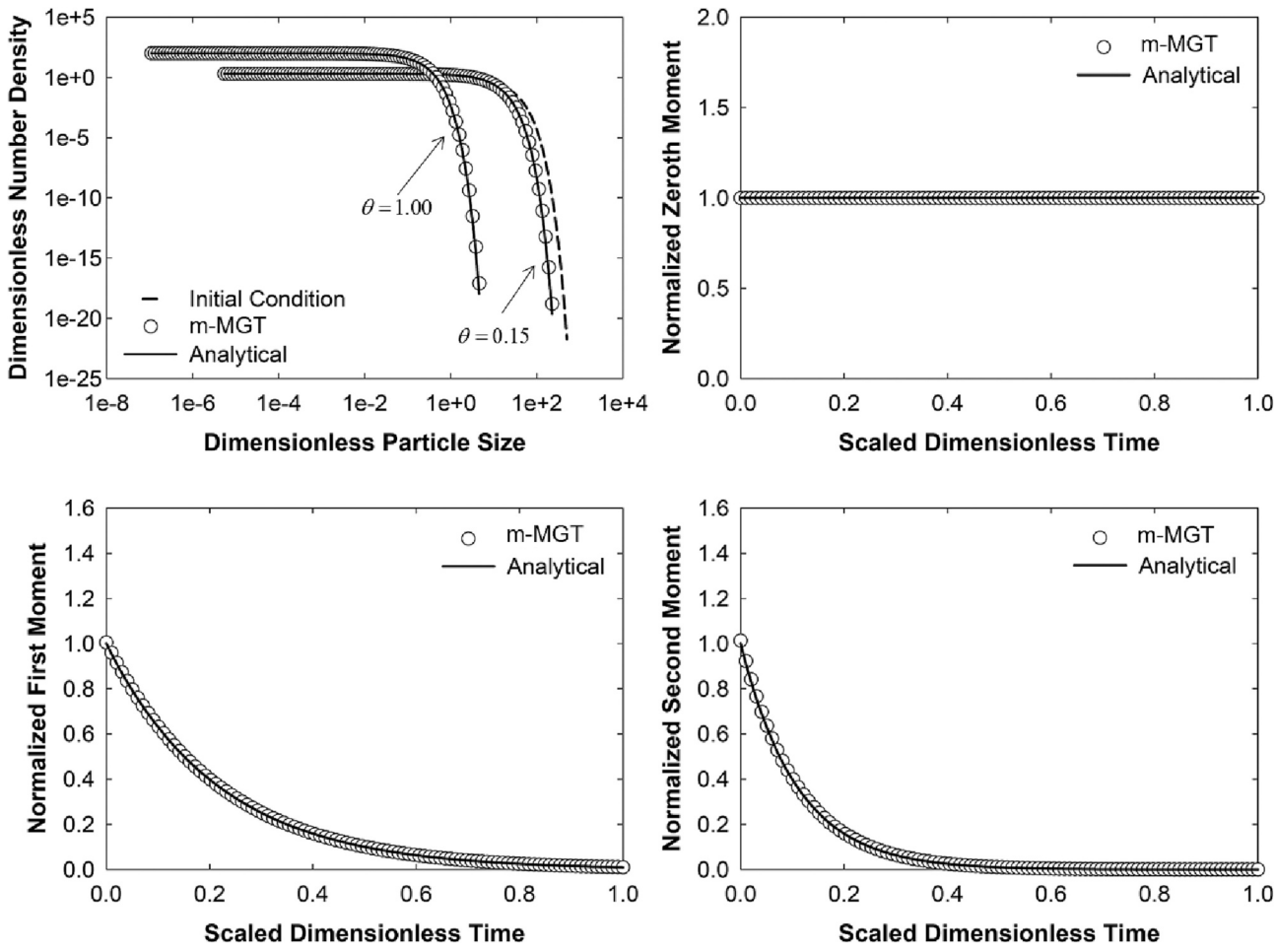

Fig. 5. Transients of: (a) the number density, (b) the zeroth moment, (c) the first moment and (d) the second moment using the m-MGT and the analytical solution for the case of pure shrinkage with a linear shrinkage rate, $c(v) = -v$. The scaled dimensionless time (θ) is normalized against the time at which 99% of the initial mass of the system is lost. The number density distributions are plotted at around 50% and 99% mass loss, i.e., $\theta = 0.15$ and $\theta = 1$ respectively. Here, a geometric grid with 100 points and $r = 1.1940$ is employed. The number of bins remains constant throughout the simulation.

order moment is given as:

$$\mu_k(t) = \int_0^\infty v^k n(v,t)dv = \sum_{i=1}^{M} x_i^k N_i \tag{11}$$

To vividly visualize the temporal evolution of the system, we normalize the k-th moment against their respective initial moment, i.e., $\mu_k(t)/\mu_k(0)$. Similarly, we also present the results in scaled dimensionless time, $\theta = t/t_{99\%}$, where $t_{99\%}$ is the time at which 99% of the initial mass of system is exhausted.

We also employ a global error indicator to quantify the discrepancy between numerical and analytical results:

$$\phi_g = \frac{1}{F}\sum_{j=1}^{F}\sum_{i=1}^{M(t_j)}\frac{1}{M(t_j)}\frac{\left|n_i^{\text{Anal}}(t_j) - n_i^{\text{m-MGT}}(t_j)\right|}{1 + n_i^{\text{Anal}}(t_j)} \tag{12}$$

where F is the total number of time steps and $M(t_j)$ is the total number of bins at each time step. Note that $M(t_j)$ is a time-independent constant in the absence of dissolution where the bins are not steadily removed. This global error reflects either the average relative error or the average absolute error over the entire period of simulation, depending on the magnitude of the analytical solutions [12]. Since the bin-discarding strategy essentially reduces the number of grid points characterizing the process, it is also crucial to determine the error at certain instances as well. To achieve this, we simply transform Eq. (12) to the following form:

$$\phi_\chi = \sum_{i=1}^{M(t_j)}\frac{1}{M(t_j)}\frac{\left|n_i^{\text{Anal}}(t_j) - n_i^{\text{m-MGT}}(t_j)\right|}{1 + n_i^{\text{Anal}}(t_j)} \tag{13}$$

where different values in the place of the subscript χ is used to denote the percentage of mass loss at the computed instance. In addition, the average relative error for the kth-order moments is computed as follows:

$$\psi_k = \frac{1}{F}\sum_{j=1}^{F}\frac{\left|\mu_k^{\text{Anal}}(t_j) - \mu_k^{\text{m-MGT}}(t_j)\right|}{\mu_k^{\text{Anal}}(t_j)} \tag{14}$$

Using the error indicators above, we assess the performance of our method late in the process after 99% of the total mass of the system is exhausted ($\theta = 1$) such that all numerical errors would have accumulated significantly. Moreover, we also investigate the rate of convergence of the m-MGT by showing the log-log plots of the global error against the initial number of bins, in which the slope indicates the rate of convergence. Additionally, we assess the error in the initial first moment of the particle population to quantify the error due to discretization of the continuous particle size domain:

$$\phi_{\text{D}} = \frac{\left|\left[\sum_{i=1}^{M(0)} x_i N_i(0)\right] - \mu_1(0)\right|}{\mu_1(0)} \tag{15}$$

The error in the initial first moment due to discretization based on our

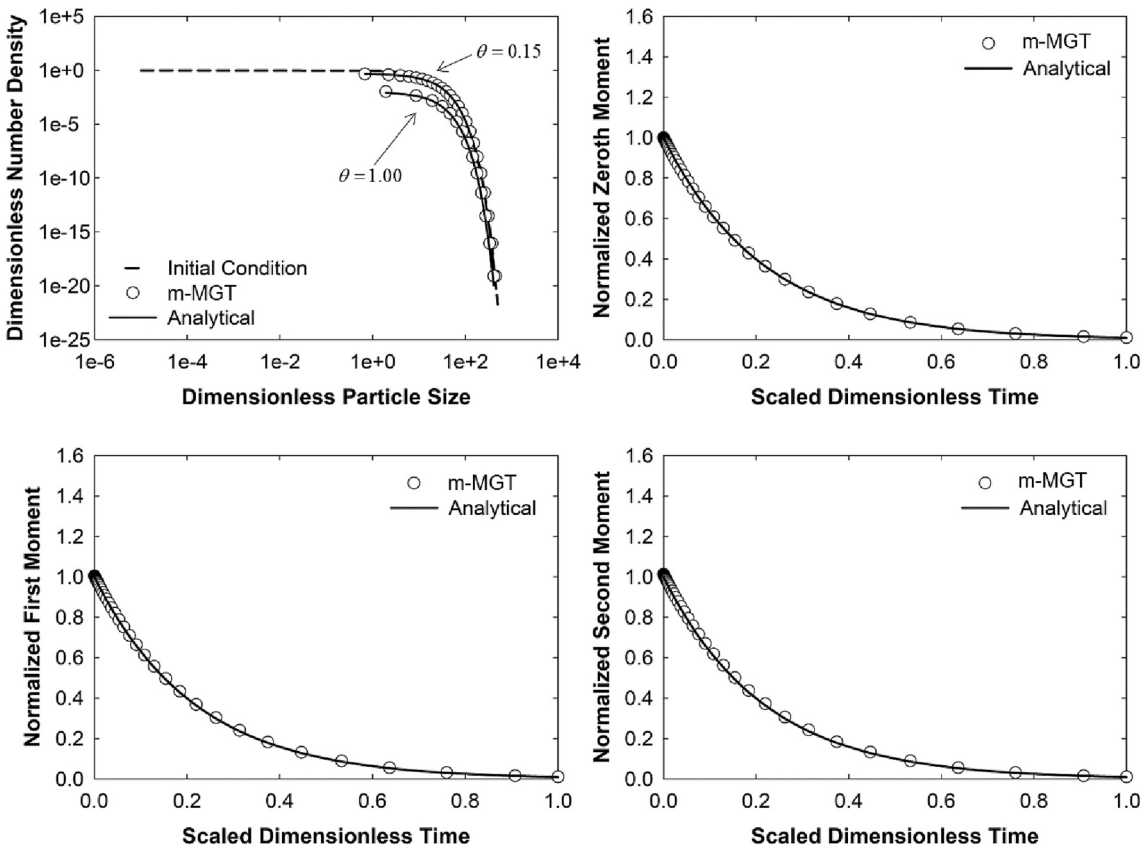

Fig. 6. Transients of: (a) the number density, (b) the zeroth moment, (c) the first moment and (d) the second moment using the m-MGT and the analytical solution for the case of simultaneous shrinkage and dissolution with a constant shrinkage rate, $c(v) = -1$. The scaled dimensionless time (θ) is normalized against the time at which 99% of the initial mass of the system is lost. The number density distributions are plotted at around 50% and 99% mass loss, i.e., $\theta = 0.15$ and $\theta = 1$ respectively. Here, a geometric grid with 100 initial points and $r = 1.1940$ is employed. The numbers of remaining bins at $\theta = 0.15$ and $\theta = 1$ are 24 and 14 respectively.

meshing configuration is generally insignificant, i.e., $\phi_D \sim O(10^{-3})$.

Lastly, all simulations in this study were executed using a workstation equipped with an AMD Ryzen 73750H processor with a clock speed of 2.30 GHz and 12 GB of installed memory (RAM). Integration of the system of ODEs in the m-MGT formulation was performed using the 'ode15s' subroutine in MATLAB® 2021a. Non-negativity of the solution was guaranteed by imposing the 'NonNegative' option of the ode subroutine.

3.2.1. Pure shrinkage

We first examine the m-MGT for the simplest case, that is, pure shrinkage through the implementation of a linear shrinkage rate function, $c(v) = -v$ (Table 1). The analytical solution for this case is obtained using the method of characteristics:

$$n(v,t) = \frac{N_0}{v_{0,i}} exp\left[-\frac{v exp(t)}{v_{0,i}}\right] exp(t) \tag{16}$$

Here, the characteristic of the pure shrinkage phenomenon is apparent through its zeroth moment:

$$\mu_0(t) = \int_0^\infty \frac{N_0}{v_{0,i}} exp\left[-\frac{v exp(t)}{v_{0,i}}\right] exp(t)\, dv = N_0 \tag{17}$$

where the total number of particles in the system does not evolve with time, implying that dissolution does not occur. The use of a linear shrinkage rate function with respect to particle size (Table 1) forces the large particles to shrink rapidly while smaller particles shrink at negligible rates, leading to a pure shrinkage phenomenon even at a very late phase. The m-MGT, in the absence of breakage ($\beta(v,w) = 0$) and dissolution, is solved through only the system of equations given by Eqs. (4) and (5).

Fig. 5(a) shows the evolution of the number density with scaled dimensionless time. The result shows that the transients of the number density are in excellent agreement with the analytical solution, with $\phi_g \sim O(10^{-4})$. The range of the PSD contracts with time as expected due to the rapid shrinkage of larger particles, although the PSD range appears not to change on a logarithmic scale. Moreover, the PSD shifts to the left with time as expected due to shrinkage but also shifts upward due to the accumulation of smaller particles as a result of their slow shrinkage with no dissolution. Fig. 5(b)-(d) also show that the m-MGT predicts the zeroth, first and second moments accurately. The temporal profile of the zeroth moment suggests that the choice of the point of dissolution, which is three orders of magnitude smaller than the initial minimum particle size, is apt as the total particle count remains constant until the very late phase of the process. The deviation of the zeroth moment from the analytical result is negligible, with $\psi_0 \sim O(10^{-6})$, whereas the average relative errors for the first and second moments are slightly higher at about $\sim O(10^{-3})$ and $\sim O(10^{-2})$, respectively, but nonetheless negligible. Lastly, as dissolution does not play a role here, the total number of bins remains constant throughout the simulation.

3.2.2. Simultaneous shrinkage and dissolution

Here, we examine the m-MGT for simultaneous shrinkage and dissolution phenomenon. The constant shrinkage rate function, $c(v) = -1$, inherently introduces an additional level of complexity due to the existence of the dissolution phenomenon (Table 1), where small particles shrink rapidly and dissolve as they approach minimum size threshold, while larger particles shrink slower relatively to their sizes

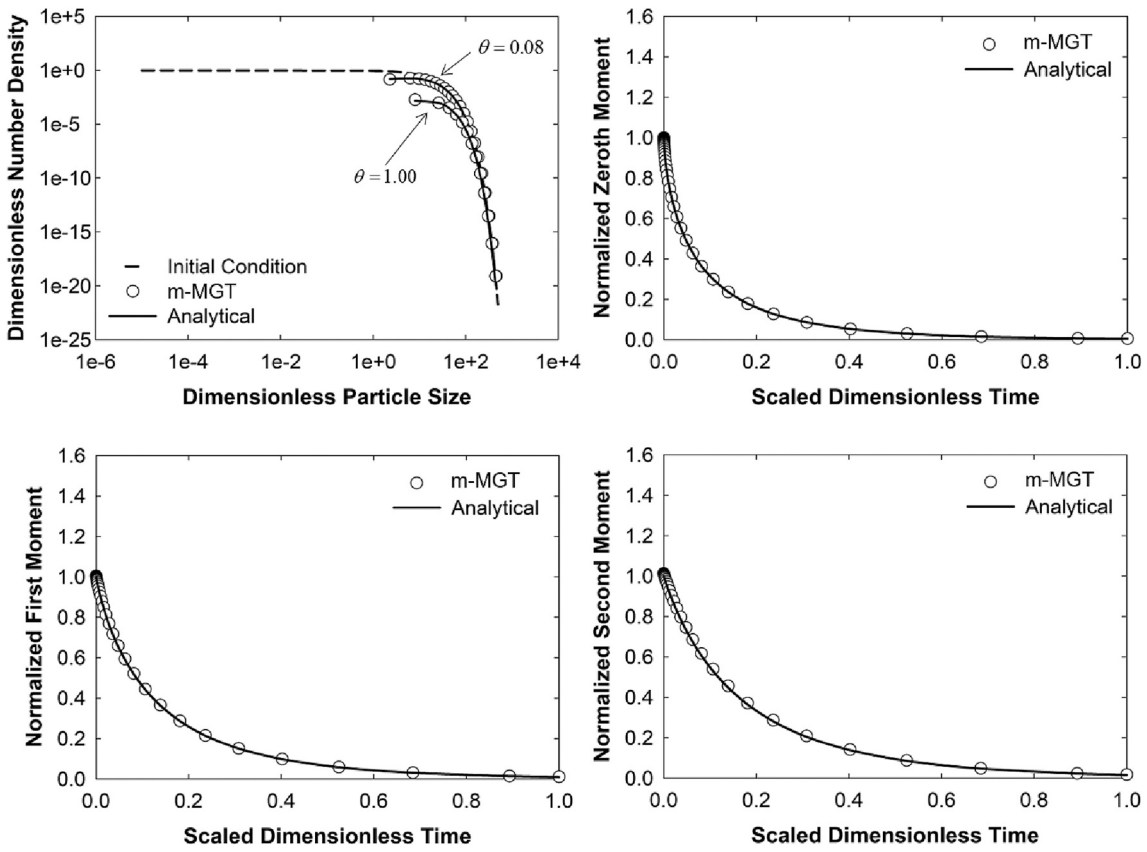

Fig. 7. Transients of: (a) the number density, (b) the zeroth moment, (c) the first moment and (d) the second moment using the m-MGT and the analytical solution for the case of simultaneous shrinkage and dissolution with a power law shrinkage rate, $c(v) = -v^{-0.5}$. The scaled dimensionless time (θ) is normalized against the time at which 99% of the initial mass of the system is lost. The number density distributions are plotted at around 50% and 99% mass loss, i.e., $\theta = 0.08$ and $\theta = 1$ respectively. Here, a geometric grid with 100 initial points and $r = 1.1940$ is employed. The numbers of remaining bins at $\theta = 0.08$ and $\theta = 1$ are 22 and 13 respectively.

and remain mostly unchanged. The analytical solution for this case is again obtained using the method of characteristics:

$$n(v,t) = \frac{N_0}{v_{0,i}} exp\left(-\frac{v+t}{v_{0,i}}\right) \tag{18}$$

The m-MGT, in the absence of breakage, only requires solution for the system of equations given by Eqs. (4) and (5), in conjunction with the removal of bins due to dissolution.

Since dissolution happens in this case, it is crucial to talk about the number of remaining bins throughout the simulation. Fig. 6(a) shows the temporal evolution of the PSD at different dimensionless times. At $\theta = 0.15$, the instance at which about 50% of the initial mass is exhausted, a total of 76 bins (i.e., >75% of the initial number of bins) have been removed due to the rapid dissolution of smaller particles. This is expected as a typical geometric grid with more points covering the small size ranges is employed in our study. At $\theta = 1$, there are only 14 bins left. Despite the minimal number of bins left in both instances, the results show that the number density profiles predicted by the m-MGT are in excellent agreement with the analytical results, with $\phi_g \sim O(10^{-4})$. Alternatively, one can easily design special meshes that are selectively refined at the larger size ranges such that more grid points will be retained at the later stages of the simulations to offer better predictions. However, this was not an issue in our case study because the average errors computed by Eq. (13) at the intermediate ($\theta = 0.15$) and late stages are also negligible, at about $\sim O(10^{-4})$. In contrast to the linear shrinkage function, the particle size distribution in this case only narrowed marginally, owing to the slow shrinkage of large particles. In addition, no smaller particles accumulate in this case because the small particle population vanishes from the system due to rapid shrinkage and subsequent dissolution. As for the moments of interest shown in Fig. 6 (b)-(d), good predictions are observed in the transient of the zeroth moment, with $\psi_0 \sim O(10^{-4})$ whereas the predictions of the temporal changes of first and second moments are also satisfactory, with average relative errors of about $\sim O(10^{-3})$ and $\sim O(10^{-2})$, respectively.

Further, the use of a general power-law shrinkage rate function, $c(v) = -v^{\gamma}$, also leads to dissolution given that $\gamma < 1$ (Table 1). The analytical solution for the shrinkage function above is:

$$n(v,t) = \frac{N_0}{v_{0,i} v^{\gamma}} \left[(1-\gamma)t + v^{1-\gamma}\right]^{\frac{\gamma}{1-\gamma}} exp\left\{-\frac{\left[(1-\gamma)t + v^{1-\gamma}\right]^{\frac{1}{1-\gamma}}}{v_{0,i}}\right\} \tag{19}$$

For the assessment with the presence of dissolution, we set $\gamma = -0.5$. Fig. 7(a) shows the temporal evolution of PSD at different times. At $\theta = 0.08$, the instance at which around 50% of the mass is exhausted, a total of 78 bins have been removed and only 13 bins are left at the end of the simulation. Similarly, the results show that the particle number density profiles obtained using the m-MGT are again in close agreement with the analytical results, with $\phi_g \sim O(10^{-4})$. Fig. 7(b)-(d) further show that the predictions of the moments of interest are satisfactory. As for the zeroth and first moments, the average relative errors are at about $\sim O(10^{-3})$. The average relative error for the second moment is slightly higher, with $\psi_2 \sim O(10^{-2})$. A careful comparison of the results between the power law and the constant shrinkage functions reveals that the small particles in the power law case shrink faster than that in the constant shrinkage case. This causes the total number of particles for the power law case to deplete at a faster rate, as seen in Fig. 6(b) and Fig. 7(b). The simulation results thus suggest that our m-MGT robustly handles various power-law shrinkage functions.

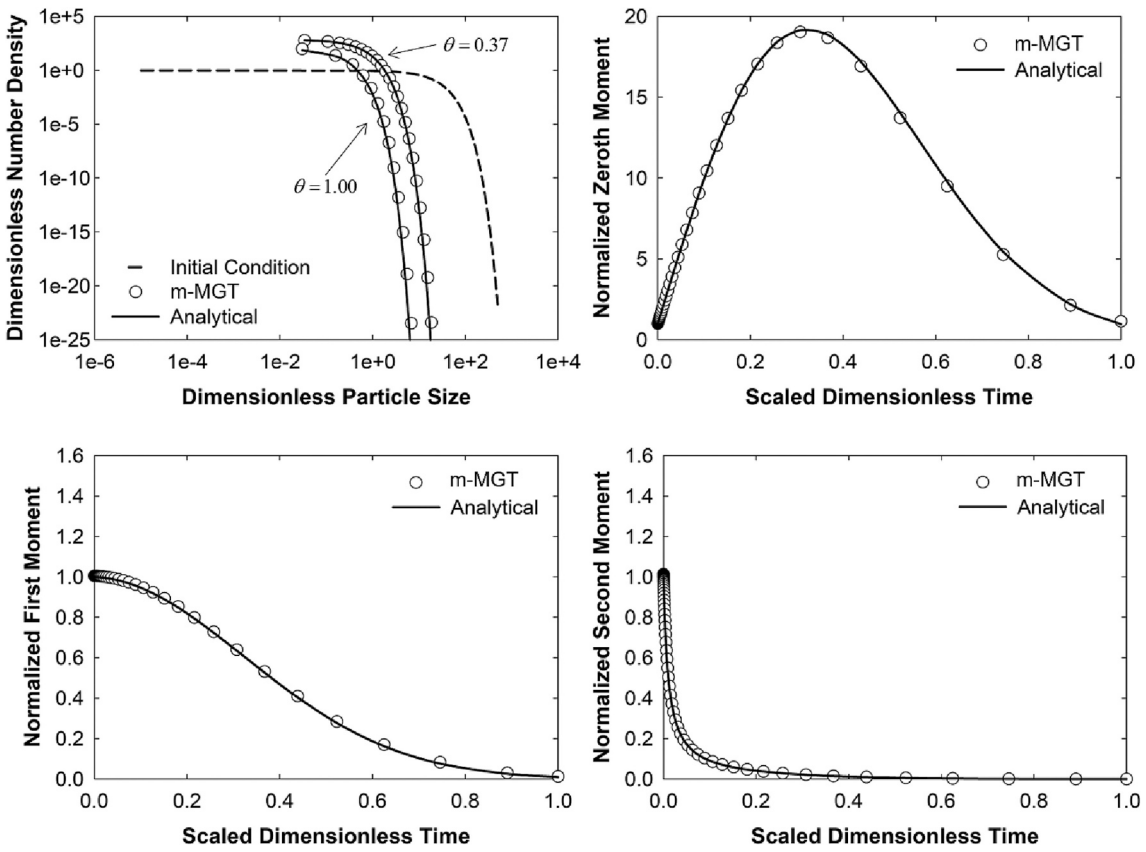

Fig. 8. Transients of: (a) the number density, (b) the zeroth moment, (c) the first moment and (d) the second moment using the m-MGT and the analytical solution for the case of simultaneous shrinkage, dissolution and breakage with a constant shrinkage rate, $c(v) = -0.1$, breakage rate, $\Gamma(v) = v$ and stoichiometric kernel, $\beta(v, w) = 2/w$. The scaled dimensionless time (θ)is normalized against the time at which 99% of the initial mass of the system is lost. The number density distributions are plotted at around 50% and 99% mass loss, i.e., $\theta = 0.37$ and $\theta = 1$ respectively. Here, a geometric grid with 100 initial points and $r = 1.1940$ is employed. The numbers of remaining bins at $\theta = 0.37$ and $\theta = 1$ are 41 and 36 respectively.

3.2.3. *Simultaneous shrinkage, dissolution and breakage*

Here, we test the capability of the m-MGT in solving simultaneous shrinkage, dissolution and breakage problem. Using the results by Huang, Edwards and Levine [5] for a constant shrinkage rate, linear breakage rate and random binary breakage stoichiometric kernel, the following analytical solution can be obtained for an initial distribution of Eq. (10):

$$n(v,t) = \frac{N_{0,i}}{v_{0,i}} exp\left(-0.5\varepsilon t^2 - vt - \frac{v+\varepsilon t}{v_{0,i}} \right) \left[t^2 v_{0,i}^2 + 2tv_{0,i} + 1 \right] \tag{20}$$

When $\varepsilon = 0$, the above expression reduces to the solution for mass-conserving breakage [37]. In addition, the conditions given by the aforementioned kernels yield the so-called recession regime, in which shrinkage is more prominent in causing the size reduction of smaller particles than breakage and leads to the rapid dissolution of smaller particles [5].

We examine the m-MGT in handling the simultaneous shrinkage, dissolution and breakage with different values of the dimensionless parameter ε, which dictates the importance of shrinkage relative to breakage. We first consider a small value of $\varepsilon = 0.1$, where the breakage phenomenon is dominant over shrinkage. Fig. 8(a) shows that the m-MGT satisfactorily predicts the transients of the number density, with $\phi_g \sim O(10^{-3})$. The number density distribution is shifted to the left, which is due to the extensive size reduction of particle population by breakage. As for the number of remaining bins, there are 41 and 36 bins remaining at $\theta = 0.37$ and $\theta = 1$ respectively. Similarly, $\theta = 0.37$ is the instance at which 50% of the initial mass is removed from the system.

Moreover, Fig. 8(b)-(d) also indicate that the temporal evolutions of all three moments are adequately predicted, with $\psi_0 \sim O(10^{-3})$ and ψ_1 and $\psi_2 \sim O(10^{-2})$. Interestingly, the total number of particles in the system increases initially and then starts dropping after 40% of the mass of the system is depleted. Such a condition is due to the inherent characteristics of the recession regime. The increase in the total number of particles indicates that the effect of breakage is indeed profound at the initial phase, where many large particles are present in the system. The reduction in particle number at the later stage is due to the rapid dissolution of small particles produced from the breakage events.

Next, we consider a shrinkage dominant process by imposing a large value on ε, i.e., 100, such that the shrinkage effect is more significant than breakage, with the same mesh setting. Fig. 9(a) again shows that the number density profiles are accurately captured, with $\phi_g \sim O(10^{-4})$. The numbers of leftover bins at $\theta = 0.23$ and $\theta = 1$ are 26 and 18 respectively. Fig. 9(b)-(d) indicate that the m-MGT satisfactorily predicts the transient of the moments of interest as well. The error for the zeroth moment is $\sim O(10^{-3})$ whereas the errors for the first and second moments are slightly higher, at about $\sim O(10^{-2})$. The monotonic reduction in the zeroth moment shows that the effect of breakage is insignificant.

The results presented in this section demonstrate that the m-MGT accurately captures the transients of simultaneous shrinkage, dissolution, and breakage process even to the very extreme cases, i.e., shrinkage dominant or breakage significant processes. Despite the number of bins decreasing with time, the numerical solutions provided by the m-MGT are still highly accurate due to the contraction of particle size range

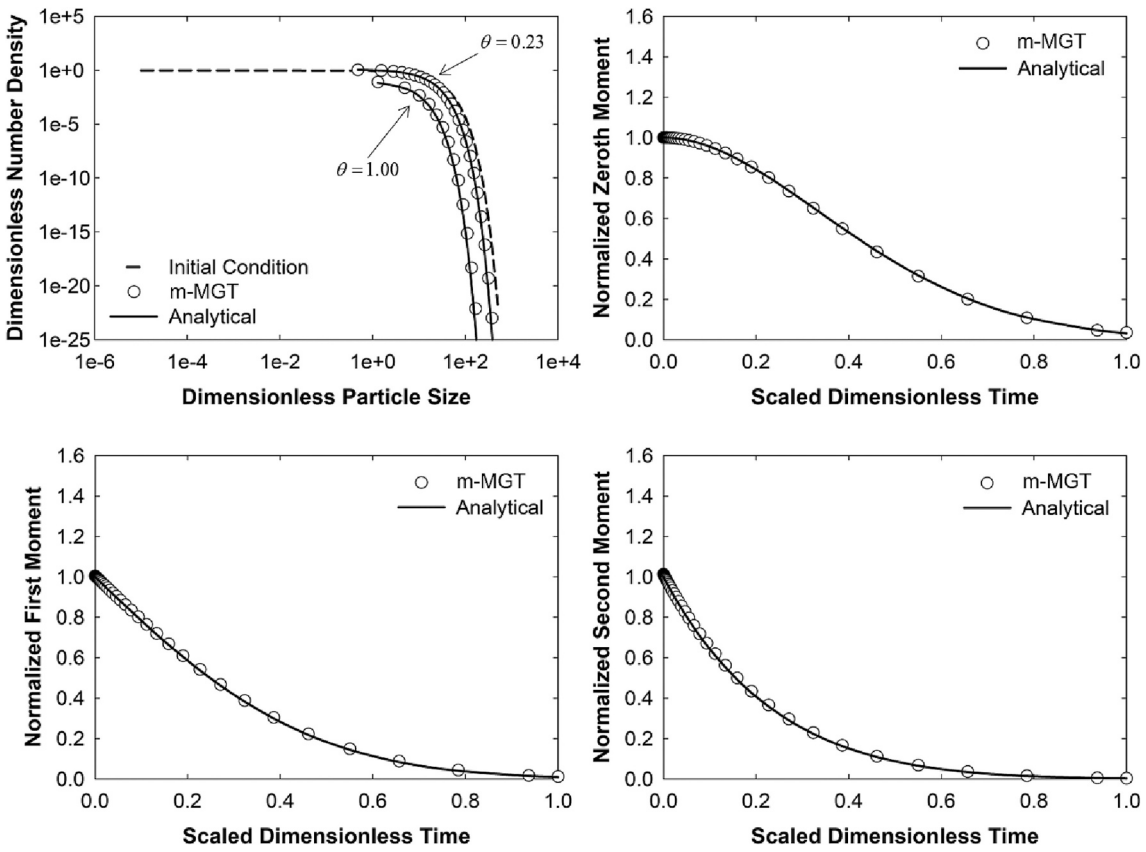

Fig. 9. Transients of: (a) the number density, (b) the zeroth moment, (c) the first moment and (d) the second moment using the m-MGT and the analytical solution for the case of simultaneous shrinkage, dissolution and breakage with a constant shrinkage rate, $c(v) = -100$, breakage rate, $\Gamma(v) = v$ and stoichiometric kernel, $\beta(v, w) = 2/w$. The scaled dimensionless time (θ)is normalized against the time at which 99% of the initial mass of the system is lost. The number density distributions are plotted at around 50% and 99% mass loss, i.e., $\theta = 0.23$ and $\theta = 1$ respectively. Here, a geometric grid with 100 initial points and $r = 1.1940$ is employed. The numbers of remaining bins at $\theta = 0.37$ and $\theta = 1$ are 26 and 18 respectively.

Table 2
Number of remaining bins and error at about 50% mass loss and $\theta = 1$, global errors for number density (ϕ_g) and average relative moment errors (ψ_0, ψ_1, ψ_2) of the m-MGT over a geometric mesh with 100 initial grid points and $r = 1.1940$.

Case study	Number of remaining bins at about 50% mass loss	Number of remaining bins at $\theta = 1$	ϕ_g	ψ_0	ψ_1	ψ_2
a) Pure shrinkage – linear shrinkage rate	100 ($\phi_{-50\%} = 1.08\times10^{-4}$)	100 ($\phi_{99\%} = 9.12\times10^{-4}$)	3.71×10^{-4}	1.00×10^{-6}	5.20×10^{-3}	1.32×10^{-2}
b) Simultaneous shrinkage and dissolution – constant shrinkage rate	24 ($\phi_{-50\%} = 2.23\times10^{-4}$)	14 ($\phi_{99\%} = 1.80\times10^{-4}$)	1.17×10^{-4}	9.46×10^{-4}	9.40×10^{-3}	1.72×10^{-2}
c) Simultaneous shrinkage and dissolution – power law shrinkage rate	22 ($\phi_{-50\%} = 7.32\times10^{-4}$)	13 ($\phi_{99\%} = 3.93\times10^{-4}$)	4.48×10^{-4}	1.65×10^{-3}	6.43×10^{-3}	1.46×10^{-2}
d) Simultaneous shrinkage, dissolution and breakage – breakage dominant	41 ($\phi_{-50\%} = 5.80\times10^{-3}$)	36 ($\phi_{99\%} = 2.50\times10^{-2}$)	2.66×10^{-3}	5.77×10^{-3}	1.40×10^{-2}	2.27×10^{-2}
e) Simultaneous shrinkage, dissolution and breakage – shrinkage dominant	26 ($\phi_{-50\%} = 5.81\times10^{-4}$)	18 ($\phi_{99\%} = 9.17\times10^{-4}$)	2.11×10^{-4}	2.34×10^{-3}	1.18×10^{-2}	2.03×10^{-2}

caused by dissolution. Table 2 summarizes the number of remaining bins and errors at about 50% mass loss and $\theta = 1$, global errors for number density and average relative moment errors of the m-MGT for all the assessed cases on a geometric mesh with an initial amount of 100 grid points and $r = 1.1940$.

3.2.4. Order of convergence

In this section, we examine the order of convergence of the m-MGT by plotting the global error against the initial number of bins for all case studies on a logarithmic scale. The order of convergence is simply the magnitude of the slopes. From Fig. 10, the m-MGT shows at least first order convergence for all the case studies. Moreover, all cases except the power law shrinkage rate demonstrates a near second order convergence.

4. Conclusion

Numerical modeling of particle dynamics in simultaneous shrinkage, dissolution and breakage requires special consideration given the number and mass-expending phenomena on the lower end of the size distribution spectrum. Using our m-MGT framework, which accounts for the convective shrinkage term and removal of size grids to represent dissolution, we assess the solution of population balances for the simultaneous shrinkage, dissolution and breakage phenomena across various scenarios (a variety of shrinkage rate functions, with/without dissolution and breakage, varying dominance between shrinkage and

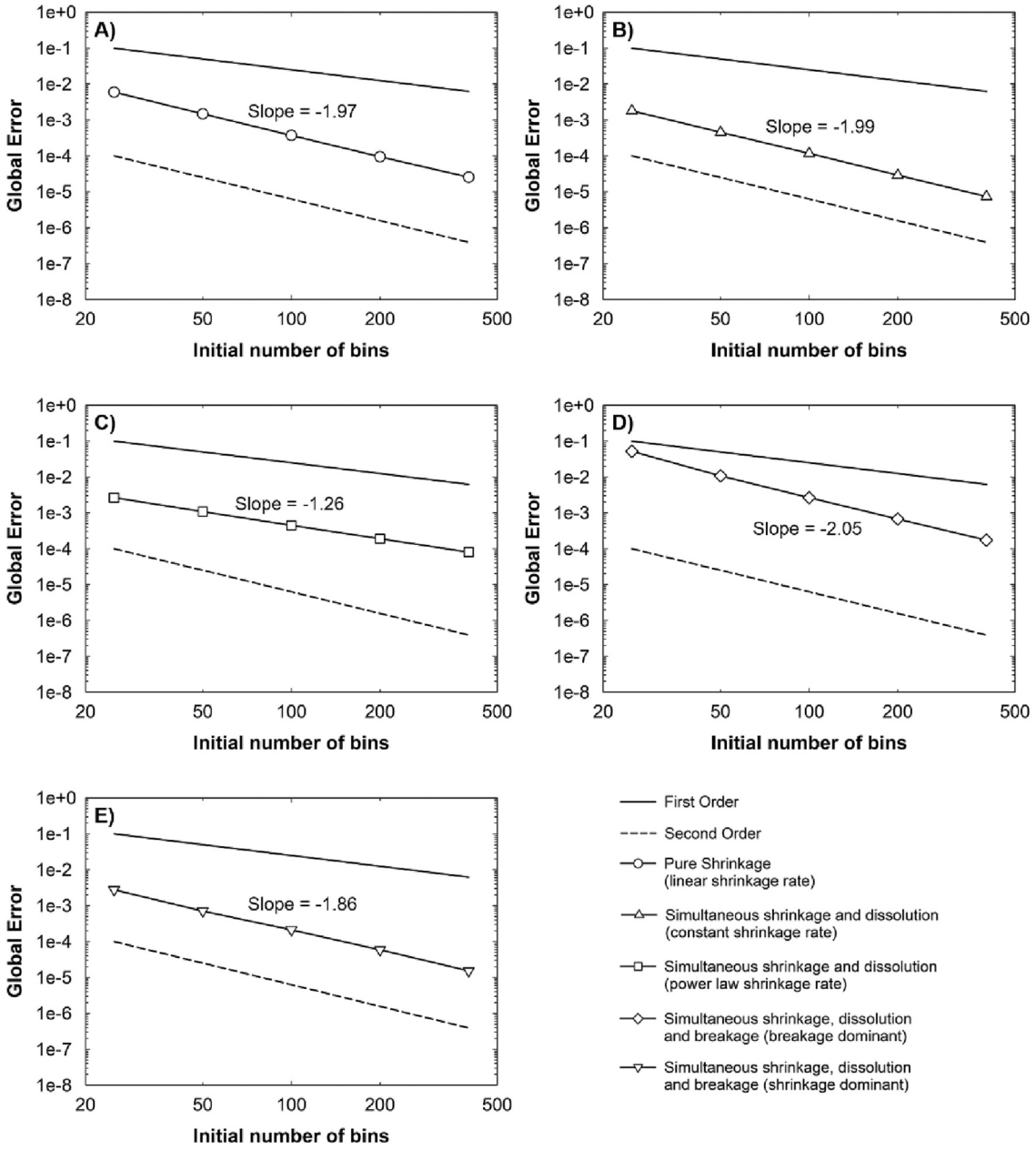

Fig. 10. Global error vs. the initial number of bins for: A) Pure shrinkage – linear shrinkage rate, B) Simultaneous shrinkage and dissolution – constant shrinkage rate, C) Simultaneous shrinkage and dissolution – power law shrinkage rate, D) Simultaneous shrinkage, dissolution and breakage – breakage dominant case, and E) Simultaneous shrinkage, dissolution and breakage – shrinkage dominant case. First and second order grid convergence are given as references.

breakage). Our approach offers adequately accurate approximations of number density profiles and moments of different orders in all assessed cases when benchmarked against established analytical solutions. As a key component of our solution technique, the stepwise removal of representative sizes on the lower end of the spectrum accurately represents the particle dissolution as seen from the decent predictions of the zeroth moment, especially for cases involving distributions with dense populations at the small size ranges. Moreover, the comparisons of the average errors evaluated at around 50% and 99% mass loss, as well as the global error reveals that our solution technique maintains accuracy over the course of the simulation despite the severe depletion of bins over time. We also demonstrate that the m-MGT exhibits at least first-order convergence for all the assessed cases. Our study ultimately shows that appropriate modification of the Moving Grid technique is essential to offer precise representations of the size-diminishing processes. Lastly, it remains to see how the m-MGT would fare in dealing with multidimensional problems and the inclusion of size-expanding phenomena such as growth and aggregation, which may pose significant challenges when resolved concurrently.

Nomenclature

Latin symbols

A	Breakage rate coefficient
B	Shrinkage rate coefficient
$\widetilde{c}(\widetilde{v})$	Shrinkage rate for particles of size $\widetilde{v}$
$c(v)$	Dimensionless shrinkage rate for particles of size v
F	Total number of time steps
$\widetilde{n}(\widetilde{v},\widetilde{t})$	Number density
$n(v,t)$	Dimensionless number density
n_i	Number density of particles of size i

η_{ik}	Particle allocation function for birth terms
N_i	Total population of the i-th bin
N_0	Initial number of particles
m	Total number of simulations/time steps after $t_{\text{shrinkage}}$
$M(t_j)$	Total number of size ranges for each time step
$\widetilde{t}$	Time
$\widehat{t}$	Scaling factor for time
t	Dimensionless time
$t_{99\%}$	Time for 99% mass loss
$t_{100\%}$	Time for 100% mass loss
t_{end}	Final simulation time
$t_{\text{shrinkage}}$	Time period before dissolution occurs
v_i, v_{i+1}	Lower and upper boundaries for the ith size range
$v_{0,i}$	Dimensionless mean size of the initial particle size distribution
$\widetilde{v}$	Particle size
$\widehat{v}$	Scaling factor for particle size
v	Dimensionless particle size
x_i	Representative size for the ith bin

Greek symbols

α	Power for the breakage rate
$\widetilde{\beta}(\widetilde{v},\widetilde{w})$	Breakage stoichiometric kernel
$\beta(v,w)$	Dimensionless breakage stoichiometric kernel
$\delta(x)$	Dirac-delta function
ε	Dimensionless factor that governs the importance of shrinkage corresponding to breakage
ϕ_g	Global error in the number density
ϕ_χ	Average error in the number density at certain instance
γ	Power for the shrinkage rate
$\widetilde{\Gamma}(\widetilde{v})$	Breakage frequency for a particle of size v
$\Gamma(v)$	Dimensionless breakage frequency for a particle of size $\widetilde{v}$
Γ_k	equivalent to $\Gamma(x_k)$
μ_k	Moment of order k
θ	Scaled dimensionless time
ψ_k	Average relative error for the kth-order moment

CRediT authorship contribution statement

Simon Ing Xun Tiong: Writing – original draft, Conceptualization, Formal analysis, Data curation, Investigation, Methodology, Software. **Firnaaz Ahamed:** Writing – review & editing, Conceptualization. **Hariswaran Sitaraman:** Writing – review & editing. **Suet Lin Leong:** Writing – review & editing. **Yong Kuen Ho:** Supervision, Project administration, Funding acquisition, Writing – review & editing.

Declaration of Competing Interest

The authors declare that they have no known competing financial interests or personal relationships that could have appeared to influence the work reported in this paper.

Data availability

Data and all MATLAB codes will be made available on request.

Acknowledgements

We would like to acknowledge the financial support in the form of Fundamental Research Grant Scheme (FRGS/1/2020/TK0/MUSM/03/1) from the Ministry of Higher Education Malaysia (MOHE), of which Yong Kuen Ho is the principal investigator. This work was authored in part by the National Renewable Energy Laboratory, operated by Alliance for Sustainable Energy, LLC, for the U.S. Department of Energy (DOE) under Contract No. DE-AC36-08GO28308. Funding provided by U.S. Department of Energy Office of Energy Efficiency and Renewable Energy Bio Energy Technologies Office. The views expressed in the article do not necessarily represent the views of the DOE or the U.S. Government. The U.S. Government retains and the publisher, by accepting the article for publication, acknowledges that the U.S. Government retains a nonexclusive, paid-up, irrevocable, worldwide license to publish or reproduce the published form of this work, or allow others to do so, for U.S. Government purposes.

Appendix A. Non-dimensionalization of PBE

The general continuous dimensional PBE for simultaneous shrinkage, dissolution and breakage problem is given as

$$\frac{\partial \widetilde{n}(\widetilde{v},\widetilde{t})}{\partial \widetilde{t}}+\frac{\partial}{\partial \widetilde{v}}\left[\widetilde{c}(\widetilde{v})\widetilde{n}(\widetilde{v},\widetilde{t})\right]=\int_{\widetilde{v}}^{\infty}\widetilde{\beta}(\widetilde{v},\widetilde{w})\widetilde{\Gamma}(\widetilde{w})\widetilde{n}(\widetilde{w},\widetilde{t})d\widetilde{w}-\widetilde{\Gamma}(\widetilde{v})\widetilde{n}(\widetilde{v},\widetilde{t}) \tag{A.1}$$

Here, $\widetilde{\Gamma}(\widetilde{v})$ is the rate kernel which describes the breakage rate of a particle with size of $\widetilde{v}$, $\widetilde{\beta}(\widetilde{v},\widetilde{w})$ is the stoichiometric kernel that governs the formation of particle with size $\widetilde{v}$ and $\widetilde{w}-\widetilde{v}$ from $\widetilde{w}$, and $\widetilde{c}(\widetilde{v})$ is the shrinkage rate for particles of size $\widetilde{v}$, which is always negative due to size reduction. As mentioned in the foregoing section, the classical power law form of rate kernels was employed in this study. The dimensional breakage rate kernel is given as $\widetilde{\Gamma}(\widetilde{v})=A\widetilde{v}^{\alpha}$ and the dimensional shrinkage rate is given as $\widetilde{c}(\widetilde{v})=-B\widetilde{v}^{\gamma}$, where $\widetilde{c}(\widetilde{v})$ is always negative due to shrinkage.

Following Cai, Edwards and Han [8], the following dimensionless variables were defined:

$$v=\frac{\widetilde{v}}{\widehat{v}} \tag{A.2}$$

$$t=\frac{\widetilde{t}}{(A\widehat{v}^{\alpha})^{-1}}=\frac{\widetilde{t}}{\widehat{t}} \tag{A.3}$$

$$\Gamma(v)=\widehat{t}\widetilde{\Gamma}(\widetilde{v}) \tag{A.4}$$

$$\beta(v,w)=\widehat{v}\widetilde{\beta}(\widetilde{v},\widetilde{w}) \tag{A.5}$$

$$c(v)=\frac{\widehat{t}}{\widehat{v}}\widetilde{c}(\widetilde{v}) \tag{A.6}$$

$$n(v,t)=\widehat{v}\widetilde{n}(\widetilde{v},\widetilde{t}) \tag{A.7}$$

Here, $\widehat{v}$ is the scaling factor for particle size which was chosen in this work to be the initial number average size, $\widehat{t}$ is the scaling factor for time which is equivalent to the reciprocal of the breakage rate of $\widehat{v}$.

Substituting all these variables leaves the PBE unchanged except that all variables are now dimensionless.

$$\frac{\partial n(v,t)}{\partial t}+\frac{\partial}{\partial v}[c(v)n(v,t)\,]=\int_{v}^{\infty}\beta(v,w)\Gamma(w)n(w,t)dw-\Gamma(v)n(v,t) \tag{A.8}$$

By recognizing that $\widehat{t}=(A\widehat{v}^{\alpha})^{-1}$, the dimensionless breakage rate can be simplified to:

$$\Gamma(v)=v^{\alpha} \tag{A.9}$$

Using the same idea, the dimensionless shrinkage rate can also be simplified:

$$c(v)=-\varepsilon v^{\gamma} \tag{A.10}$$

where $\varepsilon=(B/A)\widehat{v}^{\gamma-\alpha-1}$governs the prominence of shrinkage relative to breakage. If breakage is absent, the expressions for the dimensionless shrinkage rate and time are different:

$$c(v)=\frac{\widetilde{c}(\widetilde{v})}{B\widehat{v}^{\gamma}} \tag{A.11}$$

$$t=-\frac{\widetilde{t}}{(-B\widehat{v}^{\gamma-1})^{-1}}=-\frac{\widetilde{t}}{\widehat{t}} \tag{A.12}$$

Substituting these expressions into the PBE without breakage yields:

$$\frac{\partial n(v,t)}{\partial t}+\frac{\partial}{\partial v}[c(v)n(v,t)\,]=0 \tag{A.13}$$

The dimensionless shrinkage rate can be simplified to:

$$c(v)=-v^{\gamma} \tag{A.14}$$

where the negative sign conveys shrinkage.

Appendix B. Derivation of discrete m-MGT equations

To derive the m-MGT formulation for the simultaneous shrinkage, dissolution and breakage problem, we first consider the general PBE given in Eq. (A.1). Since the use of power law rates and nondimensionalization leave the PBE unchanged except that all variables are dimensionless, we herein derive the discrete equations based on the dimensionless PBE given by Eq. (A.8). Differentiating the shrinkage term yields the following:

$$\frac{\partial n(v,t)}{\partial t}+c(v)\frac{\partial n(v,t)}{\partial v}+n(v,t)\frac{dc(v)}{dv}=\int_{v}^{\infty}\beta(v,w)\Gamma(w)n(w,t)dw-\Gamma(v)n(v,t) \tag{B.1}$$

where the shrinkage rate is given by:

$$c(v)=\frac{dv}{dt} \tag{B.2}$$

It is worth emphasizing again that $c(v)$ is always negative for the case of shrinkage. Substituting the shrinkage rate expression into the second term of the LHS of Eq. (B.1) gives:

$$\frac{\partial n(v,t)}{\partial t}+\frac{dv}{dt}\frac{\partial n(v,t)}{\partial v}+n(v,t)\frac{dc(v)}{dv}=\int_{v}^{\infty}\beta(v,w)\Gamma(w)n(w,t)dw-\Gamma(v)n(v,t) \tag{B.3}$$

The first two terms on the LHS of the above equation can now be simplified using the chain rule of the total derivative of the number density, which gives the following:

$$\frac{dn(v,t)}{dt}+n(v,t)\frac{dc(v)}{dv}=\int_{v}^{\infty}\beta(v,w)\Gamma(w)n(w,t)dw-\Gamma(v)n(v,t) \tag{B.4}$$

Eq. (B.4) describes the change in number density of particles with size of v perceived by an observer moving at a velocity equivalent to the shrinkage rate [30]. Because $c(v)$ is always negative, the 'motion of the observer' will be in the negative direction. The mathematical transformation presented above is called the method of characteristics. Notably, the particle size v is no longer an independent variable in this setting, as it is now a function of time due to the implementation of the total derivative. Now Eq. (B.4) is ready to be combined with the basic tenets of the FP technique to produce a reliable numerical scheme for solving Eq. (A.8).

Discretizing along the axis of particle size v, the FP discretization assumes that the particle population in the i-th bin is concentrated and characterized by a representative size x_i, i.e., $v_i<x_i<v_{i+1}$. The representative sizes, x_i and the bin boundaries $v_i$can be perceived as the observers in this context, which are considered to be moving at the shrinkage rate (Eqs. (4) and (5) in the main text). The motions of x_i and v_i explicitly indicate that they are now a function of time, but for simplicity, we do not indicate this time-dependency in the equations. From Eq. (B.4), following a similar treatment by Kumar and Ramkrishna [30], the following equation can be obtained:

$$\frac{d}{dt}\int_{v_i}^{v_{i+1}} n(v,t)dv = \int_{v_i}^{v_{i+1}}\int_{v}^{\infty} \beta(v,w)\Gamma(w)n(w,t)dw\,dv - \int_{v_i}^{v_{i+1}} \Gamma(v)n(v,t)\,dv \tag{B.5}$$

At the same time, the number density function can be mathematically expressed by:

$$n(v,t) = \sum_{i=1}^{M} N_i(t)\delta(v - x_i) \tag{B.6}$$

Unlike the pure breakage problem, here both the width and the particle count in the i-th bin can change with time.

After substituting Eqs. (B.6) into (B.5) and partitioning the birth integral from $[v_i, v_{i+1}]$ to $[x_i, x_{i+1}]$ and $[x_{i-1}, x_i]$ using the FP technique with the understanding that the grid quantities are changing with time and the total number of particles for the i-th interval is $N_i(t) = \int_{v_i}^{v_{i+1}} n(v,\ t)dv$, we obtain the discretized equations in Section 2.3. The reader can refer to Kumar and Ramkrishna [11] for more details on handling the birth term using the FP technique.

References

[1] W. Zhao, M.A. Jama, A. Buffo, V. Alopaeus, Population balance model and experimental validation for reactive dissolution of particle agglomerates, Comput. Chem. Eng. 108 (2018) 240–249.
[2] D. Mangin, E. Garcia, S. Gerard, C. Hoff, J. Klein, S. Veesler, Modeling of the dissolution of a pharmaceutical compound, J. Cryst. Growth 286 (2006) 121–125.
[3] R. Seager, A.J. Acevedo, F. Spill, M.H. Zaman, Solid dissolution in a fluid solvent is characterized by the interplay of surface area-dependent diffusion and physical fragmentation, Sci. Rep. 8 (2018) 1–17.
[4] A. Adrover, A. Velardo, M. Giona, S. Cerbelli, F. Pagnanelli, L. Toro, Structural modelling for the dissolution of non-porous ores: dissolution with sporulation, Chem. Eng. J. 99 (2004) 89–104.
[5] J. Huang, B.F. Edwards, A.D. Levine, General solutions and scaling violation for fragmentation with mass loss, J. Phys. A Math. Gen. 24 (1991) 3967.
[6] K. King, Enzymic degradation of crystalline hydrocellulose, Biochem. Biophys. Res. Commun. 24 (1966) 295–298.
[7] B.F. Edwards, M. Cai, H. Han, Rate equation and scaling for fragmentation with mass loss, Phys. Rev. A 41 (1990) 5755.
[8] M. Cai, B.F. Edwards, H. Han, Exact and asymptotic scaling solutions for fragmentation with mass loss, Phys. Rev. A 43 (1991) 656.
[9] J. Huang, X. Guo, B.F. Edwards, A.D. Levine, Cut-off model and exact general solutions for fragmentation with mass loss, J. Phys. A Math. Gen. 29 (1996) 7377.
[10] S. LeBlanc, H.S. Fogler, Population balance modeling of the dissolution of polydisperse solids: rate limiting regimes, AICHE J. 33 (1987) 54–63.
[11] S. Kumar, D. Ramkrishna, On the solution of population balance equations by discretization—I. A fixed pivot technique, Chem. Eng. Sci. 51 (1996) 1311–1332.
[12] Y.K. Ho, P. Doshi, H.K. Yeoh, G.C. Ngoh, Modeling chain-end scission using the fixed pivot technique, Chem. Eng. Sci. 116 (2014) 601–610.
[13] Y.K. Ho, P. Doshi, H.K. Yeoh, Modelling simultaneous chain-end and random scissions using the fixed pivot technique, the, Can. J. Chem. Eng. 96 (2018) 800–814.
[14] F. Ahamed, M. Singh, H.-S. Song, P. Doshi, C.W. Ooi, Y.K. Ho, On the use of sectional techniques for the solution of depolymerization population balances: results on a discrete-continuous mesh, Adv. Powder Technol. 31 (2020) 2669–2679.
[15] J. Kumar, M. Peglow, G. Warnecke, S. Heinrich, L. Mörl, Improved accuracy and convergence of discretized population balance for aggregation: the cell average technique, Chem. Eng. Sci. 61 (2006) 3327–3342.
[16] M. Singh, T. Matsoukas, G. Walker, Two moments consistent discrete formulation for binary breakage population balance equation and its convergence, Appl. Numer. Math. 166 (2021) 76–91.
[17] M. Singh, V. Ranade, O. Shardt, T. Matsoukas, Challenges and opportunities concerning numerical solutions for population balances: a critical review, J. Phys. A Math. Theor. 55 (2022), 383002.
[18] M. Singh, S. Shirazian, V. Ranade, G.M. Walker, A. Kumar, Challenges and opportunities in modelling wet granulation in pharmaceutical industry–a critical review, Powder Technol. 117380 (2022).
[19] M. Singh, G. Walker, Finite volume approach for fragmentation equation and its mathematical analysis, Numer. Algorithms 89 (2022) 465–486.
[20] M. Singh, Accurate and efficient approximations for generalized population balances incorporating coagulation and fragmentation, J. Comput. Phys. 435 (2021), 110215.
[21] M. Singh, T. Matsoukas, A.B. Albadarin, G. Walker, New volume consistent approximation for binary breakage population balance equation and its convergence analysis, ESAIM, Math. Modell. Numer. Analys. 53 (2019) 1695–1713.
[22] R. Kumar, J. Kumar, G. Warnecke, Moment preserving finite volume schemes for solving population balance equations incorporating aggregation, breakage, growth and source terms, Math. Mod. Methods Appl. Sci. 23 (2013) 1235–1273.
[23] M. Hounslow, R. Ryall, V. Marshall, A discretized population balance for nucleation, growth, and aggregation, AICHE J. 34 (1988) 1821–1832.
[24] J. Kumar, M. Peglow, G. Warnecke, S. Heinrich, An efficient numerical technique for solving population balance equation involving aggregation, breakage, growth and nucleation, Powder Technol. 182 (2008) 81–104.
[25] S. Qamar, G. Warnecke, Numerical solution of population balance equations for nucleation, growth and aggregation processes, Comput. Chem. Eng. 31 (2007) 1576–1589.
[26] S. Qamar, G. Warnecke, M.P. Elsner, On the solution of population balances for nucleation, growth, aggregation and breakage processes, Chem. Eng. Sci. 64 (2009) 2088–2095.
[27] M. Singh, H.Y. Ismail, T. Matsoukas, A.B. Albadarin, G. Walker, Mass-based finite volume scheme for aggregation, growth and nucleation population balance equation, Proc. Royal Soc. A 475 (2019) 20190552.
[28] A. Majumder, V. Kariwala, S. Ansumali, A. Rajendran, Lattice Boltzmann method for population balance equations with simultaneous growth, nucleation, aggregation and breakage, Chem. Eng. Sci. 69 (2012) 316–328.
[29] Q. Hu, S. Rohani, A. Jutan, New numerical method for solving the dynamic population balance equations, AICHE J. 51 (2005) 3000–3006.
[30] S. Kumar, D. Ramkrishna, On the solution of population balance equations by discretization—III. Nucleation, growth and aggregation of particles, Chem. Eng. Sci. 52 (1997) 4659–4679.
[31] M. Strumendo, H. Arastoopour, Solution of PBE by MOM in finite size domains, Chem. Eng. Sci. 63 (2008) 2624–2640.
[32] A.L. Dale, G.V. Lowry, E.A. Casman, Accurate and fast numerical algorithms for tracking particle size distributions during nanoparticle aggregation and dissolution, Environ. Sci. Nano 4 (2017) 89–104.
[33] C. Yuan, F. Laurent, R. Fox, An extended quadrature method of moments for population balance equations, J. Aerosol Sci. 51 (2012) 1–23.
[34] D. Bertin, I. Cotabarren, J. Piña, V. Bucalá, Population balance discretization for growth, attrition, aggregation, breakage and nucleation, Comput. Chem. Eng. 84 (2016) 132–150.
[35] S. Wu, E.K. Yapp, J. Akroyd, S. Mosbach, R. Xu, W. Yang, M. Kraft, A moment projection method for population balance dynamics with a shrinkage term, J. Comput. Phys. 330 (2017) 960–980.
[36] J. Herrnring, B. Sundman, P. Staron, B. Klusemann, Modeling precipitation kinetics for multi-phase and multi-component systems using particle size distributions via a moving grid technique, Acta Mater. 117053 (2021).
[37] R.M. Ziff, E. McGrady, The kinetics of cluster fragmentation and depolymerisation, J. Phys. A Math. Gen. 18 (1985) 3027.